Static and rf magnetic field effects on fluxon dynamics in semiannular Josephson junctions

P. D. Shaju[1,*] and V. C. Kuriakose[2,†]
[1]*Department of Physics, Christ College, Irinjalakuda 680125, India*
[2]*Department of Physics, Cochin University of Science and Technology, Cochin 682 022, India*
(Received 28 October 2003; revised manuscript received 1 April 2004; published 25 August 2004)

Long semiannular Josephson junctions coupled to in-plane external static and rf magnetic fields are investigated analytically and numerically. A spatially homogeneous dc magnetic field applied in the plane of the dielectric barrier and perpendicular to a plane containing the junction boundaries induces a potential well in which trapped fluxons are pinned in the absence of a bias current. An applied rf field produces phase-locked fluxon motion manifesting constant voltage steps in the current-voltage characteristics. Analytical expressions obtained for depinning current, power-balance velocity, phase-locking range, and constant voltage steps using perturbational analysis are found to be in very good agreement with the numerical results. The proposed device is suitable for studying quantum dynamics of fluxons trapped in a potential well and in the fabrication of devices like submillimeter-wave local oscillators and constant-voltage standard devices, etc.

DOI: 10.1103/PhysRevB.70.064512 PACS number(s): 74.50.+r, 85.25.Cp, 05.45.Yv

I. INTRODUCTION

Theoretical and experimental investigations of fluxon dynamics in long superconducting tunnel junctions are currently active subjects as the well-established classical fluxon dynamics[1,2] and the currently pursuing quantum dynamics[3–5] find various applications in superconducting quantum electronic devices. Flux quanta (fluxon or Josephson vortex) in long Josephson junctions (LJJ) have the characteristics of solitons—nonlinear localized waves that preserve their shape with time—and propagate as elastic particles.[6] Fluxons, endemic to LJJs, have been employed in the fabrication of devices like constant voltage standards,[7] flux-flow oscillators,[8] current rectifiers,[9,10] logic gates,[11,12] and recently in qubits.[13,14]

LJJs of different geometries under various internal and external conditions have been investigated in the past.[15] Linear[1,8,16] and annular[17–19] LJJs subjected to in-plane static[20–22] and rf[23–25] magnetic fields are studied and various fluxon dynamical properties like fluxon trapping,[26] fluxon pinning,[27] and phase-locked states[28–30] are established theoretically and experimentally. Apart from these uniform geometries, nonuniform geometries,[31] nonrectangular geometries,[32] heart-shaped geometries,[13] semiannular and quarter-annular geometries[33] are also investigated to find further applications.

In recent times, studies have been focused on the influence of field-induced potentials on the flux motion in LJJs. Influences of field-induced sinusoidal potential in annular junctions[20] and saw-tooth potential in a modified annular junction[10] are already experimentally verified. A heart-shaped geometry[13] is used to achieve a field-induced double-well potential for demonstration of a fluxon qubit. Semiannular and quarter-annular geometries with magnetic fields applied in the plane of the dielectric barrier have been investigated to obtain magnetic field-induced tilted potentials useful for applications in bidirectional oscillators, current rectifiers, and in rf magnetic field rectifiers.[33]

The previous works on semiannular junctions[33] were based on an external magnetic field applied parallel to the dielectric barrier and parallel to a plane containing the junction boundaries. In that configuration, the effective magnetic field at the ends of the junction has opposite polarities which support penetration of opposite polarity fluxons into the junction in the presence of a forward biased current, and the junction is found to be suitable for fabrication of fluxon-based diodes for rectification of ac signals and rf magnetic fields. Working of a bidirectional flux-flow oscillator was also demonstrated for experimental realization. In this work, we investigate a semiannular junction under in-plane static and rf magnetic fields applied perpendicular to a plane containing the junction boundaries. It is found that a dc magnetic field induces a potential well which can be used for pinning the trapped fluxons in the junction. In this configuration, the external magnetic field is linked only with the interior of the junction and not with the boundaries of the junction. Therefore, the number of fluxons trapped in the junction is conserved and the system is ideal for studying quantum dynamics of trapped fluxons and in the studies of the characteristics of a nonlinear oscillator. When the junction is irradiated with an rf magnetic field, phase-locked fluxon motion with constant voltage steps are observed in the current-voltage characteristics (IVC). Different frequencies of the applied field induce different voltage steps on the IVC and the junction acts as a frequency to voltage transducer.

The paper is organized as follows. In Sec. II, we obtain the dynamical equations describing the junction in a dc magnetic field. Simple perturbational analysis is carried out to find expressions for field-induced potential well, power-balance velocity, and fluxon depinning current in the junction. In Sec. III, we formulate the theoretical model describing the junction in an rf magnetic field and obtain expressions for field-induced harmonically oscillating potential in the junction. An expression for phase-locking (PL) range is also obtained using perturbational analysis. It is found that in the phase-locked state, the fluxon moves at a constant velocity determined by the frequency of the magnetic field. In Sec. IV, details of the numerical simulations carried out to find the dc voltage characteristics, dependence of depinning current, and critical currents on magnetic fields,

 ©2004 The American Physical Society

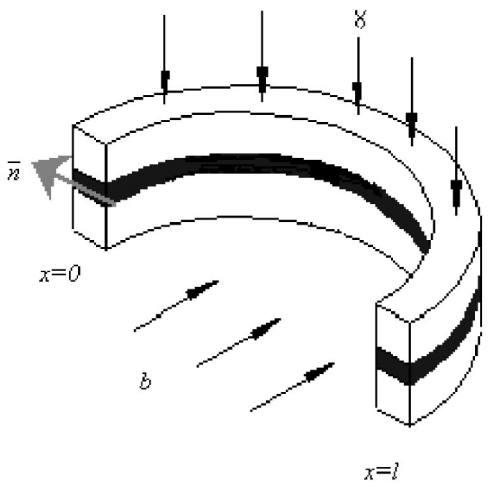

FIG. 1. A sketch of a semiannular LJJ with an applied magnetic field b parallel to the plane of the dielectric barrier of uniform thickness and perpendicular to a plane containing the junction boundaries (not drawn to scale). $\overline{n}$ represents the direction of the magnetic moment of a trapped fluxon.

rf current-voltage characteristics, and dependence of constant voltage steps on the frequencies of the applied field are presented. All the analytical results obtained are compared with numerical values and very good agreement is found. Major results of this work and conclusions are presented in Sec. V.

II. DYNAMICAL EQUATIONS IN A STATIC MAGNETIC FIELD

An LJJ with a semiannular shape is considered with an external magnetic field applied parallel to the dielectric barrier of uniform thickness and perpendicular to a plane containing the junction boundaries (Fig. 1). The direction of the applied field is indicated by arrows and the trapped fluxon's magnetic moment is represented using the unit vector $\overline{n}$. A uniform dc bias is applied across the superconducting electrodes to drive the fluxons (dc bias exerts Lorentz force on the trapped fluxons). The external field interacts with the interior of the junction and induce currents in closed form across the junction which has a net zero value over the length of the junction. The flux linked with the junction is $d\varphi(x) = (\Delta\overline{B}\cdot\overline{n})dx = \Delta B\cos[kx-(\pi/2)]dx$, where $\overline{B}$ is the strength of the applied magnetic field, $\Delta = 2\lambda_L$ is the effective penetration depth of the magnetic field into the junction, λ_L is the London penetration depth of the superconducting electrodes, $k = \pi/l$ is the normalized spatial periodicity of the magnetic field inside the semiannular junction determined by the shape of the junction, and $l = L/\lambda_J$ ($l \gg 1$) is the normalized length of the junction normalized to Josephson penetration depth λ_J. Therefore, the boundary conditions of the junction are

$$\varphi_x(0,t) = \varphi_x(l,t) = 0 \tag{1}$$

Under these conditions, a semiannular LJJ in a static magnetic field is modeled with the general perturbed sine-Gordon (sG) partial differential equation[1,32,33]

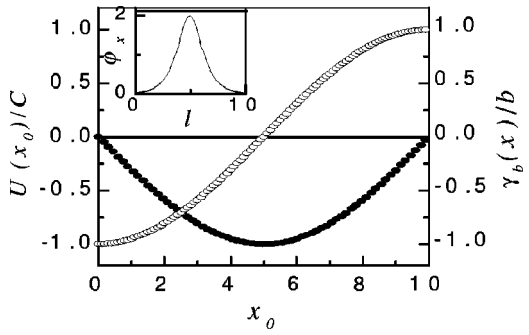

FIG. 2. The potential well $U(x_0)/C$ in the junction as a function of the fluxon coordinate x_0 (●) and the field-induced bias term $\gamma_b(x)/b$ (○) in a junction of $l=10$ at $\gamma=0$. Inset shows spatial profile (φ_x) of a trapped fluxon pinned at the center of the junction.

$$\varphi_{tt} - \varphi_{xx} + \sin\varphi = -\frac{\partial}{\partial x}(\Delta\overline{B}\cdot\overline{n}) - \alpha\varphi_t + \beta\varphi_{xxt} - \gamma, \tag{2}$$

where $\varphi(x,t)$ is the superconducting phase difference between the electrodes of the junction, the spatial coordinate x is normalized to λ_J, the time t is normalized to the inverse plasma frequency ω_0^{-1}, $\omega_0 = \tilde{c}/\lambda_J$, $\tilde{c}$ is the maximum velocity of the electromagnetic waves in the junction, $\alpha = 1/\omega_0 RC$ is the dissipation parameter due to quasiparticle current, $\beta = \omega_0 L_p/R$ is a surface damping term due to quasiparticle surface current, R is resistance per unit length, L_p is inductance per unit length, C is capacitance per unit length, and $\gamma = j/j_0$ is the normalized amplitude of a dc bias normalized to maximum Josephson current j_0. Various normalizations are discussed in Refs. 16, 32, and 33. For a homogeneous static magnetic field, the perturbed sG equation becomes

$$\varphi_{tt} - \varphi_{xx} + \sin\varphi = -b\cos(kx) - \alpha\varphi_t + \beta\varphi_{xxt} - \gamma, \tag{3}$$

with $b = 2k(B/B_{c1})$, where $B_{c1} = \Phi_0/\pi\Lambda\lambda_J$ is the first critical penetration field for an LJJ and $\Phi_0 = h/2e = 2.064\times10^{-15}$ Wb is the flux quantum. Compared with the standard sG model for Josephson junctions,[1] this equation has an extra term, $\gamma_b(x) = -b\cos(kx)$ (see Fig. 2), which corresponds to a spatially reversing field-induced driving force on the fluxons reversing at the center of the junction. This force exerts a transient force on the trapped fluxons and locates them at the center of the junction. Thus, in the absence of a bias current, fluxons are pinned by the external magnetic field in the junction.

On neglecting the small perturbations ($\alpha=\beta=\gamma=b=0$), Eq. (3) becomes the sG equation with the soliton solution[2]

$$\varphi(x,t) = 4\tan^{-1}\left[\exp\frac{\sigma(x-x_0)}{\sqrt{1-u^2}}\right], \tag{4}$$

where $x_0 = ut + x_0'$ is the instantaneous location, u is the normalized velocity, $\sigma = \pm 1$ is the polarity, and x_0' is the initial position of the soliton. The soliton solution corresponds to a vortex of supercurrent, which carries a magnetic field of a single flux quantum Φ_0 (fluxon) localized around ut and traveling with the velocity u. In the classical regime, a fluxon is considered as a nonrelativistic particle with rest mass $m_0 = 8$, moving in one dimension.

A. Expression for the potential well

In order to obtain an expression for the field-induced potential well, we first calculate the Lagrangian density of Eq. (3) with $\alpha=\beta=\gamma=0$ as

$$\mathbf{L}=\frac{\varphi_t^2}{2}-\frac{1}{2}\left(\varphi_x-\frac{b}{k}\sin(kx)\right)^2-1+\cos\varphi, \tag{5}$$

where the first term represents the kinetic energy associated with the energy density of the electric field, the second term accounts for the potential energy density associated with the magnetic field, and the third term represents the Josephson coupling energy density. Therefore, the change in potential energy density due to the applied field can be determined from the second term of the above equation

$$\mathbf{U}(x)=\frac{1}{2}\left\{\varphi_x^2-\frac{2b}{k}\sin(kx)\varphi_x+\left(\frac{b}{k}\sin(kx)\right)^2\right\}. \tag{6}$$

In the above equation, the first term is independent of the applied field and the third term is independent of the fluxon motion in the junction. Therefore, the change in the potential due to the combined effect of fluxon motion and the applied field can be determined by integrating the second term of the above equation over the length of the junction. Since the length of the junction is very large compared to the size of the fluxon, integration can be extended from $-\infty$ to $+\infty$. Results obtained in infinitely long junctions can be applied to finite length junctions with fairly good accuracy.[1] Hence, the fluxon-induced potential as a function of fluxon coordinate x_0 is calculated as

$$U(x_0)=-\frac{b}{k}\int_{-\infty}^{+\infty}\sin(kx)\varphi_x dx. \tag{7}$$

Substituting Eq. (4) in (7) and integrating, we get an expression for the potential

$$U(x_0)=-2bl\,\mathrm{sech}\left(\frac{\pi^2}{2l}\sqrt{1-u^2}\right)\sin(kx_0). \tag{8}$$

At velocities $u\simeq 0$, the above equation reduces to

$$U(x_0)=-C\sin(kx_0), \tag{9}$$

where $C=2bl\,\mathrm{sech}(\pi^2/2l)$ is a constant. The potential well $U(x_0)$, field-induced driving term $\gamma_b(x)$, and the spatial profile of a single fluxon φ_x trapped in the junction are shown in Fig. 2. The applied field induces a potential well in the junction with potential minimum located at the point where the fluxon's magnetic moment is directed along the external field. In this model, the potential minimum is located at the center of the junction. Thus, using semiannular geometry, fluxons can be pinned at the center of the junction and the geometry may find application in studying quantum dynamics of fluxons.

B. Power-balance velocity

To find the power-balance velocity, we first make an energy balance analysis and determine the instantaneous rate of change of fluxon velocity. The power-balance analysis pioneered by McLaughlin and Scott[1] is applicable to infinite length junctions. In semi-infinite length junctions at low damping, it is assumed that fluxons attain the steady-state velocity on moving a distance equal to the length of the junction.

Energy of the unperturbed sG system is

$$H^{\mathrm{sG}}=\int_{-\infty}^{\infty}\left[\frac{1}{2}(\varphi_t^2+\varphi_x^2)+1-\cos\varphi\right]dx. \tag{10}$$

Inserting Eq. (4) in Eq. (10) and integrating, we get the energy of a fluxon moving with velocity u as $H^{\mathrm{sG}}=8/\sqrt{1-u^2}$. Therefore, the rest energy of a fluxon in normalized units is 8. Perturbational parameters modulate the velocity of the fluxon and may cause dissipation of energy. The rate of dissipation is calculated by computing

$$\frac{d}{dt}(H^P)=[\varphi_x\varphi_t]_{-\infty}^{\infty}-\int_{-\infty}^{\infty}[\alpha\varphi_t^2+\beta\varphi_{xt}^2+(b\cos(kx)+\gamma)\varphi_t]dx, \tag{11}$$

where the first term on the right side accounts for the boundary conditions and vanishes. Inserting Eq. (4) in Eqs. (11) and making an energy balance analysis, we get

$$\frac{du}{dt}=\frac{\pi}{4}\gamma(1-u^2)^{3/2}-\alpha u(1-u^2)-\frac{1}{3}\beta u+\frac{\pi}{4}b(1-u^2)^{3/2}\,\mathrm{sech}\left[\frac{\pi^2\sqrt{1-u^2}}{2l}\right]\cos(kx_0). \tag{12}$$

This expression describes the effects of perturbations on the fluxon velocity. In the above equation, the first term on the right-hand side represents the input power from the bias current, the second and third terms represent energy dissipation due to internal damping, and the fourth term accounts for the effect of the external field.

At higher bias values, energy input to a fluxon is balanced with the energy loss due to dissipation and the fluxon moves at constant velocity (u_c). Therefore, the rate of change of fluxon velocity over a period can be taken as zero. The steady velocity u_c of a fluxon over a period T is given by $u_c=2l/T$ In the steady state, average rate of change of fluxon velocity over a period T is calculated as $\int_0^T(du/dt)dt=0$. Integrating Eq. (12) over a period $T=2l/u_c$ we see that the last term on the right-hand side vanishes, and we obtain

$$\frac{\pi}{4}\gamma(1-u_c^2)^{3/2}=\alpha u_c(1-u_c^2)+\frac{1}{3}\beta u_c. \tag{13}$$

At $\beta=0$ the power-balance velocity becomes

$$u_c=\pm\left[1+\left(\frac{4\alpha}{\pi\gamma}\right)^2\right]^{-1/2}. \tag{14}$$

In deriving the above equation, we have not taken into account the energy loss during reflection at the boundaries. Open boundary conditions affect the fluxon's steady-state velocity in two ways.[34] The intrinsic energy losses in the reflection due to the dissipation parameter α affect the steady-state velocity, and the phase shift associated with the

reflection gives a further correction to the average velocity. The energy loss due to α during a reflection is given by[35]

$$\Delta H_1 = -2\pi^2 \alpha f(u), \tag{15}$$

where $f(u)$ is a velocity-dependent function which can be approximated as $f(u)=1$ at velocities $u \sim 1$, and the phase shift produced during reflection is given by[36]

$$\delta = -2(1-u^2)^{1/2} \ln u. \tag{16}$$

In order to calculate the steady-state velocity, we have to incorporate the reflection losses ΔH_1 at one end of the junction, which is $2\pi^2\alpha$. The power delivered to a junction of length l by the bias current γ is $2\pi\gamma l$. Therefore, taking the energy loss during reflection, the effective driving term (γ') in the junction may be defined as[34]

$$2\pi\gamma' l = 2\pi\gamma l - 2\pi^2\alpha. \tag{17}$$

Substituting this effective driving term $\gamma' = \gamma - (\pi\alpha)/l$ in Eq. (14), the steady-state velocity u_c becomes

$$u_c' = \pm \left[1 + \left(\frac{4\alpha}{\pi\left(\gamma - \frac{\pi\alpha}{l} \right)} \right)^2 \right]^{-1/2}. \tag{18}$$

Finally, the phase-shift corrected steady-state velocity can be calculated as[35]

$$u_0 = u_c' \left[1 - \frac{\delta}{l} \right]^{-1}, \tag{19}$$

where δ is given by Eq. (16) with $u=u_c$. The above equation gives steady-state velocity attained by a fluxon in a semiannular junction. The energy loss during reflection at the open boundaries of the junction influences the steady-state velocity only at low bias values. At higher bias values, these corrections are small and can be neglected. Moreover, all these effects associated with the open boundary conditions will be taken automatically in the direct numerical simulation of the perturbed sG equation [Eq. (3)]. From the above expressions we see that the power-balance velocity (and hence the average voltage) is determined by the dissipation parameters and the bias current, and not by the external magnetic field. Thus, external magnetic field has no influence on the steady-state velocity of a fluxon in the junction.

C. Fluxon depinning current

At very low dc bias values, a trapped fluxon is pinned in the potential well and corresponds to zero-voltage state. Higher dc bias tilts the potential helping fluxons to move in the junction. Fluxon motion in the junction contributes for finite voltage states. The dc bias at which zero voltage switches to a finite voltage corresponds to the fluxon depinning current (γ_d). At zero-voltage state (i.e., at $u=0$ and $du/dt=0$), Eq. (12) becomes

$$\gamma = -b \operatorname{sech}\left[\frac{\pi^2}{2l} \right] \cos\theta, \tag{20}$$

where $\theta = kx_0'$ is an angular parameter which depends on the initial location of the fluxon. From the above equation we find the magnitude of the largest possible bias current for zero-voltage state (i.e., depinning current) as

$$\gamma_d = \left| b \operatorname{sech}\left(\frac{\pi^2}{2l} \right) \right|. \tag{21}$$

The threshold value for fluxon depinning is directly proportional to the strength of the magnetic field and is determined by the length of the junction. The open boundary conditions influence the zero-voltage state in the junction. When a fluxon is reflected at the open boundary, the threshold driving term γ_{th} corresponding to fluxon annihilation can be calculated by equating the incident fluxon energy with the energy loss due to reflection plus the fluxon rest energy. i.e.,

$$\frac{8}{\sqrt{1-u_c^2}} = 2\pi^2\alpha + 8. \tag{22}$$

Substituting the steady-state velocity [Eq. (14)] in the above equation, we get the approximate value of the fluxon annihilation threshold at small velocities as $\gamma_{th} = (2\alpha)^{3/2}$.[34] By incorporating the threshold for fluxon annihilation in the depinning current γ_d, we get the magnitude of the bias current for average zero-voltage state (γ_0) as

$$\gamma_0 = b \operatorname{sech}\left(\frac{\pi^2}{2l} \right) + (2\alpha)^{3/2}. \tag{23}$$

This is the applied dc bias value below which zero-voltage state exists in the junction. Above γ_d, the fluxon gets depinned in the potential well and above γ_0 the fluxon undergoes periodic motion, which corresponds to a switching of the IVC to finite voltage state from zero-voltage state. The zero-voltage locking range in the junction can be obtained from Eq. (20) by varying θ in the range $[0-\pi]$ as

$$(\Delta\gamma)_S = 2b \operatorname{sech}\left(\frac{\pi^2}{2l} \right). \tag{24}$$

The zero-voltage locking range is an important parameter in studying dynamics of fluxons in the potential well.

III. DYNAMICAL EQUATIONS IN rf MAGNETIC FIELDS

Following the methods adopted in Sec. II, the dynamical equations representing a semiannular LJJ in a harmonically oscillating magnetic field applied parallel to the dielectric barrier and perpendicular to a plane containing the junction boundaries and with a dc bias across the superconducting electrodes can be obtained from Eq. (3) as

$$\varphi_{tt} - \varphi_{xx} + \sin\varphi = -b \sin(\omega t)\cos(kx) - \alpha\varphi_t + \beta\varphi_{xxt} - \gamma, \tag{25}$$

where ω is the normalized frequency of the magnetic field normalized to the Josephson plasma frequency ω_0. As in Sec. II, the boundary conditions of the junction are

$$\varphi_x(0,t) = \varphi_x(l,t) = 0. \tag{26}$$

Details of the fluxon dynamics can be obtained by finding the potential induced by the time-varying magnetic field in

the junction and the energy change associated with the moving fluxon. The Lagrangian density of Eq. (25) with $\alpha=\beta=\gamma=0$ is

$$\mathbf{L}=\frac{\varphi_t^2}{2}-\frac{1}{2}\left(\varphi_x-\frac{b}{k}\sin(\omega t)\sin(kx)\right)^2-1+\cos\varphi. \quad (27)$$

Therefore, the corresponding potential energy density is obtained from the second term of the above equation

$$\mathbf{U}(x,t)=\frac{1}{2}\left\{\varphi_x^2-\frac{2b}{k}\sin(\omega t)\sin(kx)\varphi_x+\left(\frac{b}{k}\sin(\omega t)\sin(kx)\right)^2\right\}. \quad (28)$$

The first term is independent of the applied field and the third term is independent of the flux motion in the junction. Therefore, the change in the potential due to the combined effect of the applied field and the fluxon motion in the junction as a function of the fluxon coordinate x_0 can be determined from the second term as

$$U(x_0,t)=-\frac{b}{k}\int_{-\infty}^{+\infty}\sin(\omega t)\sin(kx)\varphi_x dx. \quad (29)$$

Substituting Eq. (4) in (29) and integrating, we get

$$U(x_0,t)=-2bl\,\mathrm{sech}\left(\frac{\pi^2}{2l}\sqrt{1-u^2}\right)\sin(\omega t)\sin(kx_0). \quad (30)$$

At velocities $u\simeq 0$, the above expression becomes

$$U(x_0,t)=-C\sin(\omega t)\sin(kx_0), \quad (31)$$

where $C=2bl\,\mathrm{sech}(\pi^2/2l)$ is a constant. Equation (31) shows that the potential is oscillating at the frequency of the applied field. This oscillating potential modulates the fluxon velocity and is responsible for the phase-locked fluxon motion in the junction.

A. Phase-locking range

To calculate the phase-locked states, we first calculate the net dissipation of energy by the perturbational parameters as

$$\frac{d}{dt}(H^P)=[\varphi_x\varphi_t]_{-\infty}^{\infty}-\int_{-\infty}^{\infty}[\alpha\varphi_t^2+\beta\varphi_{xt}^2+(b\sin(\omega t)\cos(kx)+\gamma)\varphi_t]dx. \quad (32)$$

The first term on the right side in the above equation represents the boundary conditions and vanishes. Inserting Eq. (4) in Eq. (32) and following perturbative analysis, we obtain the rate of energy dissipation as

$$\frac{d}{dt}(H^P)=2\pi\gamma u-\frac{8\alpha u^2}{\sqrt{1-u^2}}-\frac{8\beta u^2}{3(1-u^2)^{3/2}}+2\pi bu\,\mathrm{sech}\left[\frac{\pi^2}{2l}\sqrt{1-u^2}\right]\sin(\omega t)\cos(kx_0). \quad (33)$$

The above equation describes the effect of rf magnetic field in modulating the fluxon energy. In deriving the above equation, we neglected the small contribution to the energy loss during reflection at the boundaries and the phase-shift-induced correction to the fluxon energy. In phase-locked state, the fluxon executes periodic motion (at the period of the magnetic field) with constant velocity $u_0=2l/T$. The total energy in the phase-locked state remains unchanged over a period ($T=2\pi/\omega$). The net change in energy over a period T is calculated as $\int_0^T(d/dt)(H^P)dt=0$ Integrating. Eq. (33) over a period T, we get

$$\int_0^T 2\pi\gamma u_0 dt-\int_0^T\frac{8\alpha u_0^2}{\sqrt{1-u_0^2}}dt-\int_0^T\frac{8\beta u_0^2}{3(1-u_0^2)^{3/2}}dt+\int_0^T 2\pi bu_0\,\mathrm{sech}\left[\frac{\pi^2}{2l}\sqrt{1-u_0^2}\right]\sin(\omega t)\cos(kx_0)dt=0, \quad (34)$$

where $x_0=u_0t+\theta/k$. Using the values of u_0 and T, the fluxon coordinate can be expressed in terms of the frequency ω as $kx_0=\omega t+\theta$. Substituting in the above equation and integrating, we get

$$2\pi\gamma u_0-\frac{8\alpha u_0^2}{\sqrt{1-u_0^2}}-\frac{8\beta u_0^2}{3(1-u_0^2)^{3/2}}-\pi bu_0\,\mathrm{sech}\left[\frac{\pi^2}{2l}\sqrt{1-u_0^2}\right]\sin\theta=0. \quad (35)$$

Therefore, we get the following condition for PL:

$$\gamma=\frac{4\alpha u_0}{\pi\sqrt{1-u_0^2}}+\frac{4\beta u_0}{3\pi(1-u_0^2)^{3/2}}+\frac{b}{2}\,\mathrm{sech}\left[\frac{\pi^2}{2l}\sqrt{1-u_0^2}\right]\sin\theta, \quad (36)$$

where $\theta=kx_0'$. The largest dc bias for zero-voltage state can be calculated from the above equation as $(\gamma_d)_{\mathrm{rf}}=(b/2)\mathrm{sech}(\pi^2/2l)$, which is half of the fluxon depinning current in a static field. By varying θ between $-\pi/2$ and $+\pi/2$, we get the lower and upper threshold values of the bias current for PL as

$$\gamma_1=\frac{4\alpha u_0}{\pi\sqrt{1-u_0^2}}+\frac{4\beta u_0}{3\pi(1-u_0^2)^{3/2}}-\frac{b}{2}\,\mathrm{sech}\left[\frac{\pi^2}{2l}\sqrt{1-u_0^2}\right], \quad (37)$$

$$\gamma_2=\frac{4\alpha u_0}{\pi\sqrt{1-u_0^2}}+\frac{4\beta u_0}{3\pi(1-u_0^2)^{3/2}}+\frac{b}{2}\,\mathrm{sech}\left[\frac{\pi^2}{2l}\sqrt{1-u_0^2}\right]. \quad (38)$$

The threshold values are found to be symmetric around the IVC at no magnetic field. The range of PL is obtained as

$$\Delta\gamma=\gamma_2-\gamma_1=b\,\mathrm{sech}\left[\frac{\pi^2}{2l}\sqrt{1-u_0^2}\right]. \quad (39)$$

Since $u_0=2l/T=l\omega/\pi$, the above equation for PL range becomes

$$(\Delta\gamma)_{\rm rf} = b\ \mathrm{sech}\left[\frac{\pi^2}{2l}\sqrt{1-\left(\frac{\omega l}{\pi}\right)^2}\right]. \tag{40}$$

Thus, the PL range is found to be proportional to the strength of the applied field and is determined by the field frequency ω and the junction length l. The locking range is independent of the loss parameters α and β as well as the bias term γ. We note that at $u_0 \simeq 0$, the range of zero-voltage locked state in an rf field becomes

$$(\Delta\gamma)_{\rm rf} = b\ \mathrm{sech}\left[\frac{\pi^2}{2l}\right], \tag{41}$$

which is half of the zero-voltage range in a static field (24).[23]

In phase-locked state, the fluxon executes periodic motion at the frequency of the applied field with constant velocity $u \simeq u_0$ given by

$$u_0 = \frac{2l}{T} = \frac{l\omega}{\pi}. \tag{42}$$

Thus, PL velocity is determined by the frequency of the rf field and the length of the junction. Since the average velocity is proportional to the voltage across the junction, the above equation represents the frequency-voltage relation in the junction. For a single fluxon, the maximum average normalized velocity attainable is $u_0 \simeq 1$ and therefore we get the maximum value of the fundamental harmonic frequency of the rf field for PL as $\omega_0 = \pi/l$.

IV. NUMERICAL RESULTS

All analytical expressions obtained in the previous section are verified using numerical simulations. The system is simulated by solving the perturbed sG Eq. (3) using the boundary conditions of Eq. (1). For the discretization of the differential equations, we used an explicit method treating φ_{xx} with a five-point, φ_{tt} with a three-point, and φ_t with a two-point finite-difference method. A time step of 0.0125 and a space step of 0.025 is used in the discretization. The fluxon solution of Eq. (4) with zero velocity is used as the initial condition. This corresponds to a single fluxon trapped at the center of the junction. After the simulation of the phase dynamics for a transient time, we calculate the average voltage $\langle V\rangle$ for a time interval T as $\langle V\rangle = (1/T)\int_0^T \varphi_t dt = [\varphi(T) - \varphi(0)]/T$. For faster convergence of our averaging procedure, we additionally averaged the phases $\varphi(x)$ over the length of the junction. Since the mean voltage in the junction is proportional to the average velocity of the fluxon, average velocity of a fluxon is calculated using the relation $\langle u\rangle = l/2\pi\langle V\rangle = l/2\pi\langle\varphi_t\rangle$. Details of the numerical simulation procedure can be found in Refs. 12, 16, and 33.

A. IVC in a static magnetic field

The average velocities, $\langle u\rangle$, attained by a fluxon at different bias currents γ are determined in the numerical simulation, and a plot of the average velocity versus dc bias forms the IVC of the junction. In the absence of external field (at $b=0$), fluxon dynamics in semiannular LJJ is the same as that in any ordinary rectangular junction and zero-voltage state exists up to the critical value $\gamma_{th} = (2\alpha)^{3/2}$. Above γ_{th}, average velocity increases gradually from zero value as the bias is increased and finally reaches the maximum value, $u \simeq 1$. When an external magnetic field is applied, a potential well is induced in the junction and the fluxon remains pinned in the potential well as long as the Lorentz force exerted on the fluxon by the bias current is smaller than the pinning force. If the pinning force is exceeded by the driving force, the fluxon starts to move. As the fluxon gets depinned, a voltage jump from zero to finite voltage is detected. The fluxon depinning current depends on the magnitude and direction of the applied field. Thus, with external magnetic fields, greater threshold bias γ_0 is required to get finite voltages. Figure 3(a) shows the IVC of a junction with a single trapped fluxon at different magnetic fields. We have considered a junction with parameters $l=10$, $\alpha=0.05$, and $\beta=0.01$. The system is started with a single fluxon trapped at the center of the junction. Simulation started with $\gamma=0$ and then increased in very small steps up to a maximum of $\gamma=0.9$. In all cases, at sufficiently higher bias values ($\gamma > \gamma_0$), average velocity increases asymptotically and approaches the maximum velocity $u \simeq 1$ in the junction. At still higher bias values, the junction switches to resistive state with uniformly increasing nonlocalized phase values showing high voltage states.

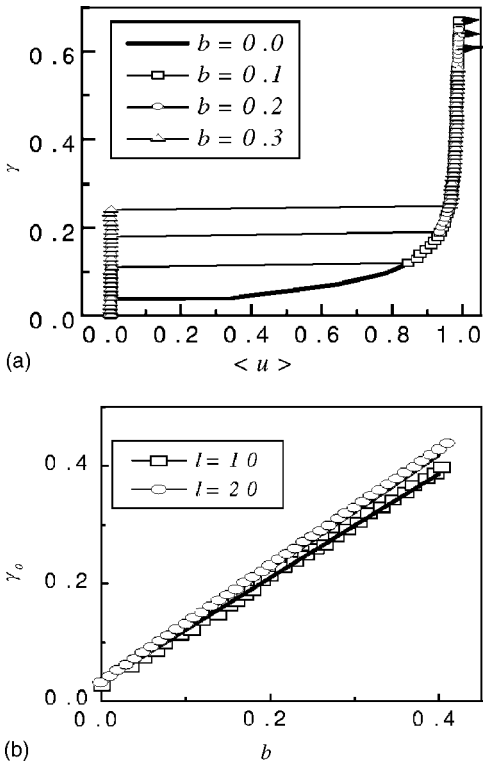

FIG. 3. (a) Applied dc bias γ versus the average velocity $\langle u\rangle = l/2\pi\langle\varphi_t\rangle$ at different values of the magnetic fields. The parameters of the junction are $l=10$, $\alpha=0.05$, and $\beta=0.01$. (b) Magnetic field intensity b versus zero-voltage bias current γ_0 showing linearity of γ_0 with b on two junctions with parameters $\alpha=0.05$ and $\beta=0$. Solid lines represent values computed using Eq. (23) and symbols represent numerical results with a single fluxon trapped in the junction.

The depinning current γ_d is found to increase linearly with the strength of the applied field due to strong pinning in

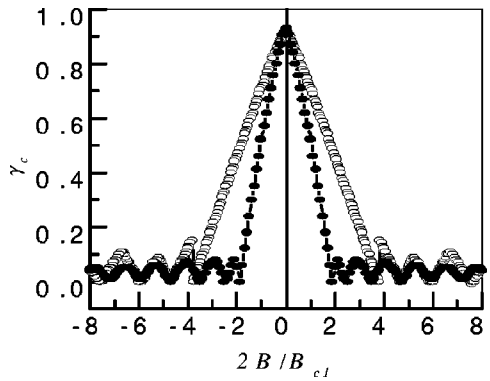

FIG. 4. Critical current (γ_c) versus static magnetic field ($2B/B_{c1}=b/k$) of a semiannular LJJ (○) and that of a rectangular LJJ (●) of $l=10$, $\alpha=0.05$, and $\beta=0$ without any trapped fluxons.

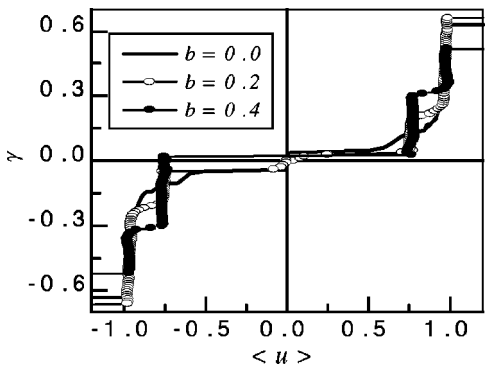

FIG. 5. IVC at different rf magnetic field intensities showing constant voltage steps. The parameters are $l=12$, $\alpha=0.05$, $\beta=0.01$, and $\omega=0.2$.

higher fields. To check the linearity of γ_d with b, the average zero-voltage bias current γ_0 calculated using Eq. (23) (solid lines) along with that obtained in numerical simulation of Eq. (3) (symbols) with a single fluxon trapped in the junction is shown in Fig. 3(b). Theoretical values match exactly with the numerical values.

B. Critical current versus magnetic field

The characteristics of an LJJ undergo drastic changes when an external magnetic field is applied. It is important for practical applications to know the behavior of the junction under a static magnetic field, especially the dependence of critical current (γ_c) on the applied field (B). In weak static magnetic fields, LJJs behave like weak superconductors and show the Meissner effect. In this regime the critical current decreases linearly with the external field. This behavior exists up to the first critical field, B_{c1}. At this critical field, magnetic flux in the form of fluxons can overcome the edge barrier effects and can penetrate the junction.[37] The dependence of γ_c on static magnetic field ($2B/B_{c1}=b/k$) applied to a semiannular LJJ of $l=10$ without any trapped fluxons is shown in Fig. 4. For comparison, critical current versus magnetic field diffraction pattern of a standard rectangular LJJ is also presented. The first critical field (B_{c1}) for fluxon penetration in semiannular junction is found to be approximately twice that in a rectangular junction. Also, from the diffraction pattern it is noticed that at all magnetic fields, critical current in semiannular junction is higher than that in a rectangular junction. This is expected as there is no flux linked at the boundaries of the junction. The higher critical field values in semiannular junction show that the junction can be easily decoupled from external fluctuations.

C. IVC in an rf magnetic field

To find the IVC of the junction in rf magnetic fields, we directly integrated Eq. (25) with the boundary conditions (26). Figure 5 shows the normalized dc bias γ versus the average velocity $\langle u \rangle$ of a single fluxon in a junction of $l=12$, $\alpha=0.05$, and $\beta=0.01$ at magnetic field amplitudes $b=0.2$ and $b=0.4$. The frequency of the rf field is taken as $\omega=0.2$. IVC without the external magnetic field ($b=0$) is also plotted to show the symmetric locking range. At $\gamma=0$, the fluxon is pinned in the potential minimum which is at the center of the junction. For bias values $[\gamma<(\gamma_d)_{\rm rf}]$, the fluxon executes oscillatory motion around the potential minimum point, contributing a net zero voltage across the junction. At higher values of the dc bias $[\gamma>(\gamma_d)_{\rm rf}]$, average velocity increases gradually and the phase-locked fluxon motion is manifested as a constant voltage step on the IVC. Constant voltage steps are observed at the steady-state velocity $u_0=(l\omega)/\pi=0.76$. The PL range is found to increase in proportion with the strength of the applied field. It is noticed that even for relatively large magnetic field amplitudes, very close agreement is found between numerically obtained constant voltage steps and analytically predicted results. On increasing the bias values further, average velocity switches to the asymptotic value $u\simeq 1$. At still higher bias values, the junction switches to resistive state showing high voltages.

D. Phase-locking range

The PL range ($\Delta\gamma/b$) as a function of the velocity parameter ω/k obtained using Eq. (40) together with the corresponding values obtained by numerical simulation of Eq. (25) in different length junctions are shown in Fig. 6. Nu-

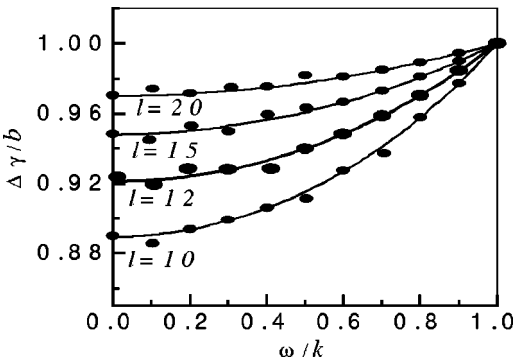

FIG. 6. PL range $\Delta\gamma/b$ as function of velocity parameter $u_0=\omega/k$. Theoretical values computed using Eq. (40) are shown (solid lines) along with numerically obtained values (●) for different length junctions. The parameters are $\alpha=0.05$, $\beta=0.01$, and $b=0.2$.

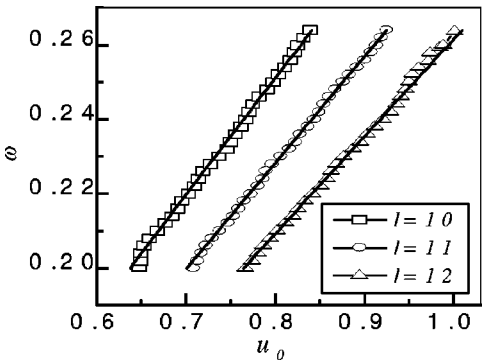

FIG. 7. rf magnetic field frequency ω as a function of the PL velocity u_0. The parameters are $\alpha=0.05$, $\beta=0.01$, $b=0.3$, and $\gamma=0.2$. Solid lines represent values computed using Eq. (42) and symbols represent numerically obtained values.

merically obtained values are shown as solid circles. The PL range is independent of dissipation parameters, so we fixed the parameters at $\alpha=0.05$ and $\beta=0.01$ and used some discrete values of the parameter ω/k in the range 0 to 1 on different length junctions. The perturbational result (40) predicts that the locking range is identical to the external magnetic field strength b at the highest velocity $\omega/k=1$ in the junction. Very good agreement is found between the perturbational method and numerical solution of the perturbed sG equation for almost all choices of parameters. Similar results were obtained earlier in annular Josephson junctions.[23]

In order to check the validity of the frequency to voltage relation (42), we numerically obtained the steady-state velocity u_0 at different frequencies of the rf field keeping all other parameters constant. In Fig. 7, PL velocities as a function of the frequency of the rf field are shown on different length junctions of $\alpha=0.05$, $\beta=0.01$, $\gamma=0.2$, and $b=0.3$. PL velocity is found to vary linearly in accordance with the relation (42). Solid lines represent values computed using Eq. (42), and symbols represent numerically obtained values. As the fundamental harmonic frequency approaches the PL frequency limit $\omega_0=\pi/l=0.261$ in a junction of $l=12$, PL velocity u_0 approaches the maximum value $u\simeq 1$. Results show that the junction acts as a frequency to voltage standard and is useful for measurement of unknown frequencies of rf fields.

V. CONCLUSION

In this work, we have studied various static and dynamical properties of a single fluxon trapped in a semiannular LJJ under in-plane static and rf magnetic fields in the classical regime. The external field contributes a spatially reversing perturbation in the interior of the junction. It is demonstrated that fluxons trapped in semiannular LJJ reside in a pinning potential well when a uniform dc magnetic field is applied parallel to the junction's tunnel barrier and perpendicular to a plane containing the junction boundaries. The height of the potential well is determined by the strength of the applied field and the dc bias applied to the junction. The system is closely analogous to an annular junction as there is no interaction of the external magnetic field with the open boundaries of the junction, and so the number of fluxons trapped in the junction is conserved. Investigations can be extended to the quantum regime to find different quantum energy states of the trapped fluxons useful for quantum computing applications. The semiannular junction in the proposed configuration is useful for investigating thermal activation and quantum tunneling properties of the fluxons. Fluxon motion is found to be phase locked under an rf magnetic field. Phase-locked state produces a constant voltage step in the IVC and the junction may find application as constant voltage standards. We have considered only the fundamental harmonic frequencies of the rf field. Analysis can be extended to find the subharmonic phase-locked states that may find application in submillimeter-wave local oscillators with potential applications in space research. More interesting dynamics can be observed when larger numbers of fluxons are trapped in the junction and also in vertically stacked junctions. Investigations under an ac bias can also be carried out to get some useful applications. Using current fabrication methods of the annular junctions and fluxon trapping techniques,[38] semiannular junctions can be easily fabricated and experimental realization becomes simple. In brief, we have proposed a method for studying quantum dynamics of fluxons in a potential well and for the fabrication of devices like constant voltage standards and submillimeter-wave local oscillators.

ACKNOWLEDGMENT

One of the authors (V.C.K.) wishes to acknowledge IUCAA, Pune.

*Email address: pds@cusat.ac.in
†Email address: vck@cusat.ac.in

[1] D. W. McLaughlin and A. C. Scott, Phys. Rev. A **18**, 1652 (1978).
[2] A. C. Scott, F. Y. F. Chu, and D. W. McLaughlin, IEEE Trans. Magn. **MAG-61**, 1443 (1973).
[3] A. Wallraff, A. Lukashenko, J. Lisenfeld, A. Kemp, M. V. Fistul, Y. Koval, and A. V. Ustinov, Nature (London) **425**, 155 (2003).
[4] A. Wallraff, T. Duty, A. Lukashenko, and A. V. Ustinov, Phys. Rev. Lett. **90**, 037003 (2003).
[5] M. H. Devoret, D. Esteve, C. Urbina, J. Martinis, A. Cleland, and J. Clarke, *Quantum Tunnelling in Condensed Media* (North-Holland, Amsterdam, 1992).
[6] A. V. Ustinov, Physica D **123**, 315 (1998).
[7] R. L. Kautz and R. Monaco, J. Appl. Phys. **57**, 875 (1985); R. L. Kautz, Appl. Phys. Lett. **36**, 386 (1980); M. T. Levinsen, R. Y. Chiao, M. J. Feldman, and B. A. Tucker, *ibid.* **31**, 776 (1977).
[8] T. Nagatsuma, K. Enpuku, F. Irie, and K. Yoshida, J. Appl. Phys.

63, 1130 (1983); V. P. Koshelets, A. V. Shchukin, S. V. Shitov, and L. V. Filippenko, IEEE Trans. Appl. Supercond. **3**, 2524 (1993).
[9] F. Raissi and J. E. Nordman, IEEE Trans. Appl. Supercond. **5**, 2943 (1995); Appl. Phys. Lett. **65**, 1838 (1994).
[10] G. Carapella and G. Costabile, Phys. Rev. Lett. **87**, 077002 (2001); G. Carapella, Phys. Rev. B **63**, 054515 (2001).
[11] Y. Nakamura, Y. A. Pashkin, and J. S. Tsai, Nature (London) **398**, 786 (1999).
[12] P. D. Shaju and V. C. Kuriakose, Phys. Lett. A **267**, 420 (2000); Physica C **322**, 163 (1999).
[13] A. Kemp, A. Wallraff, and A. V. Ustinov, Phys. Status Solidi B **233**, 472 (2002); Physica C **368**, 324 (2002); A. Wallraff, Y. Koval, M. Levitchev, M. V. Fistul, and A. V. Ustinov, J. Low Temp. Phys. **118**, 543 (2000).
[14] Y. Makhlin, G. Schön, and A. Shnirman, Rev. Mod. Phys. **73**, 357 (2001).
[15] A. Barone, and G. Paternó, *Physics and Applications of the Josephson Effect* (Wiley, New York, 1982); Yu. S. Kivshar, and B. A. Malomed, Rev. Mod. Phys. **61**, 763 (1989).
[16] P. S. Lomdahl, O. H. Soerensen, and P. L. Christiansen, Phys. Rev. B **25**, 5737 (1982).
[17] A. V. Ustinov, T. Doderer, R. P. Huebener, N. F. Pedersen, B. Mayer, and V. A. Oboznov, Phys. Rev. Lett. **69**, 1815 (1992).
[18] A. Davidson, B. Dueholm, B. Kryger, and N. F. Pedersen, Phys. Rev. Lett. **55**, 2059 (1985).
[19] A. V. Ustinov, T. Doderer, I. V. Vernik, N. F. Pedersen, R. P. Huebener, and V. A. Oboznov, Physica D **68**, 41 (1993).
[20] A. V. Ustinov and B. A. Malomed, Phys. Rev. B **64**, 020302 (2001).
[21] N. Grønbech-Jensen, P. S. Lomdahl, and M. R. Samuelsen, Phys. Rev. B **43**, 12 799 (1991).
[22] A. V. Ustinov, B. A. Malomed, and E. Goldobin, Phys. Rev. B **60**, 1365 (1999); M. V. Fistul and A. V. Ustinov, *ibid.* **63**, 024508 (2000).
[23] N. Grønbech-Jensen, P. S. Lomdahl, and M. R. Samuelsen, Phys. Lett. A **154**, 14 (1991).
[24] A. V. Ustinov and N. Thyssen, J. Low Temp. Phys. **106**, 193 (1997).
[25] M. Salerno, M. R. Samuelsen, G. Filatrella, S. Pagano, and R. D. Parmentier, Phys. Lett. A **137**, 75 (1989); Phys. Rev. B **41**, 6641 (1990).
[26] S. Keil, I. V. Vernik, T. Doderer, A. Laub, H. Preßler, R. P. Huebener, N. Thyssen, A. V. Ustinov, and H. Kohlstedt, Phys. Rev. B **54**, 14 948 (1996).
[27] I. V. Vernik, S. Keil, N. Thyssen, T. Doderer, A. V. Ustinov, H. Kohlstedt, and R. P. Huebener, J. Appl. Phys. **81**, 1335 (1997).
[28] N. F. Pedersen and A. Davidson, Phys. Rev. B **41**, 178 (1990).
[29] N. Grønbech-Jensen, Phys. Lett. A **169**, 31 (1992); M. Cirillo and F. L. Lloyd, J. Appl. Phys. **61**, 2581 (1987).
[30] N. Grønbech-Jensen and M. R. Samuelsen, Phys. Lett. A **191**, 57 (1994); R. Monaco, S. Pagano, and G. Costabile, *ibid.* **131**, 122 (1988).
[31] V. M. Krasnov, V. A. Oboznov, and N. F. Pedersen, Phys. Rev. B **55**, 14 486 (1997); A. Benabdallah, J. G. Caputo, and A. C. Scott, *ibid.* **54**, 16 139 (1996); J. Appl. Phys. **88**, 3527 (2000).
[32] E. Goldobin, A. Sterck, and D. Koelle, Phys. Rev. E **63**, 031111 (2001).
[33] P. D. Shaju and V. C. Kuriakose, Phys. Rev. B **65**, 214508 (2002); Supercond. Sci. Technol. **16**, L25 (2003); Phys. Lett. A **299**, 628 (2002); Physica C **383**, 395 (2003); Pis'ma Zh. Eksp. Teor. Fiz. **76**, 14 (2002) [Sov. Phys. JETP **76**, 14 (2002)].
[34] N. F. Pedersen, M. R. Samuelsen, and D. Welner, Phys. Rev. B **30**, 4057 (1984).
[35] O. H. Olsen, N. F. Pedersen, M. R. Samuelsen, H. Svensmark, and D. Welner, Phys. Rev. B **33**, 168 (1986).
[36] O. A. Levring, N. F. Pedersen, and M. R. Samuelsen, J. Appl. Phys. **54**, 987 (1983).
[37] C. S. Owen and D. J. Scalapino, Phys. Rev. **164**, 538 (1967).
[38] A. V. Ustinov, Appl. Phys. Lett. **80**, 3153 (2002).